NJC

Cite this: New J. Chem., 2017, 41, 4096

Design and *in vitro* biological evaluation of substituted chalcones synthesized from nitrogen mustards as potent microtubule targeted anticancer agents†

X. Janet Sabina,[a] J. Karthikeyan,*[a] Gunasekaran Velmurugan,[b] M. Muthu Tamizh[c] and A. Nityananda Shetty[d]

A new series of *p*-[*N*,*N*-bis(2-chloroethyl)amino]benzaldehyde substituted chalcone derivatives were designed and synthesized, and their structures were characterized by spectroscopic techniques and single crystal XRD studies. Compounds **3a–f** crystallized in the triclinic system with a centrosymmetric space group $P\bar{1}$, except for crystal **3c** which crystallized in the monoclinic crystal system with a centrosymmetric space group *P*21/*c*. Molecular docking studies were utilized to reveal the binding mode of the derivatives to identify new tubulin inhibitors. Density functional theory calculations were performed to understand the structural and electronic properties of these chalcones. The DFT results show that the HOMOs of all the chalcones lie in the range of −5.65 to −6.17 eV and the LUMOs in the range of −2.01 to −3.21 eV. The experimental results are well supported by the theoretical structural analysis. The biological activity of these compounds showed high potency of growth inhibitory effects with sub-micromolar IC_{50} values ranging from 0.089 to 0.200 μM against A549 and HepG2 cancer cell lines. Furthermore, these compounds exhibited a strong inhibitory effect on tubulin polymerization. **3e** showed the highest mean activity against both the cancer cells and in tubulin inhibition. This correlated well with the theoretical results from the pharmacophore binding model. Hence, these six compounds, particularly **3e**, could be considered as potential leads in the development of new anticancer agents.

Received 21st January 2017,
Accepted 18th April 2017

DOI: 10.1039/c7nj00265c

rsc.li/njc

1. Introduction

Microtubules are important cytoskeletal components consisting of α- and β-tubulin heterodimers. They are involved in various critical cellular functions such as intracellular transport, cell signalling, motility regulation and especially mitosis since microtubules are one of the key components of the mitotic spindle.[1–3] Hence, they are attractive targets for anticancer treatment. Anti-mitotic drugs basically interfere with microtubule dynamics at the G2/M phase leading to apoptotic cell death.[4,5] Microtubule inhibitors interact with tubulin through at least four well documented binding sites, namely the taxane, vinca, colchicine and laulimalide binding sites.[6–9] Paclitaxel and laulimalide induce tubulin assembly and are microtubule stabilizers, while vinca and colchicine inhibit tubulin assembly and are microtubule destabilizers.[10–13] These anti-mitotic agents have gained widespread interest due to their success in clinical oncology. However, the clinical use of some tubulin inhibitors, like colchicine, has been limited by toxicity and drug resistance. Hence, there is a real need to develop small molecules that can act as tubulin binding inhibitors, and have fewer side effects and reduced drug resistance.[5,14] This would help in better understanding microtubule dynamics and the different mechanisms of action of anticancer drugs.

Chalcones are an important group of natural products belonging to the flavonoid family. They consist of two aromatic rings connected by an α,β-unsaturated carbonyl moiety.[15,16] The natural and

[a] *Department of Chemistry, Sathyabama University, Chennai – 600119, India. E-mail: dr.j.karthikeyan@gmail.com*
[b] *Department of Chemistry, Indian Institute of Technology Bombay, Mumbai – 400076, India*
[c] *Department of Chemistry, Siddha Central Research Institute, Central Council for Research in Siddha, Arumbakkam, Chennai – 600106, India*
[d] *Department of Chemistry, National Institute of Technology Karnataka, Mangalore – 575025, India*

† Electronic supplementary information (ESI) available: Spectral data, check cif files of all chalcones (**3a–f**), packing fraction of chalcones, binding model of chalcones, MDL 27048 and colchicine with β-tubulin, pharmacophore model of the chalcones, absorbance of chalcones in the tubulin inhibition assay, DFT optimized structures, and frontier molecular orbital energies and molecular orbital composition (%) of various fragments in the ground state. CCDC 1042842, 1061656, 1035426, 1402531, 1426151 and 1426150. For ESI and crystallographic data in CIF or other electronic format see DOI: 10.1039/c7nj00265c

synthetic derivatives of chalcones and their hybrids display considerable pharmacological activity such as anti-fungal, anti-microbial, anti-malarial, anti-tubercular, anti-inflammatory, anti-diabetic, as tyrosinase and cholinesterase inhibitors, *etc.*[17–25] Chalcones have also been identified as antimitotic agents since the discovery by Edwards in 1990[26] and are known to act as anticancer agents.[27–30] Chalcones bind to the colchicine site at the interface of α- and β-tubulin heterodimers and prevent their assembly into microtubules. Anti-mitotic agents binding to the colchicine site are considered significant lead structures in the development of anticancer drugs. A number of chalcones and their derivatives have already been shown to be good antimitotic agents, the most significant being MDL 27048. Peyrot *et al.* have reported the mechanism of binding of this anti-mitotic drug to tubulin resulting in cell cycle arrest and mitosis.[31,32] Other agents that act in a similar way are combretastatin, podophyllotoxin and their analogues.[33–35] Combretastatin is a powerful anti-proliferative agent that binds to the colchicine site and inhibits tubulin polymerization.[36] Podophyllotoxin also binds at the same site but adopts a different orientation.[37]

Herein we report the biological activity of a series of chalcones synthesized from the potential anticancer agent *p*-[*N*,*N*-bis(2-chloroethyl)amino]benzaldehyde. This aldehyde contains the *N*,*N*-bis(2-chloroethyl)amino group, otherwise known as nitrogen mustard. Such compounds have frequently displayed potent activity against cancer cells.[38,39] Anticancer therapy should be based on the use of more than one compound, since combined use can increase efficacy and reduce drug resistance. The synthesis and biological activity of thiosemicarbazones and their metal complexes as well as chalcones prepared from the above aldehyde have already been reported.[40–43] The results obtained have strengthened the hypothesis that chalcones synthesized from such a potential anticancer agent should exhibit enhanced anticancer activity. Also, chalcones are structurally diverse small organic molecules having features well suited for binding macromolecules. Their simplicity of synthesis, the possibility of synthesizing a large number of derivatives and their significant pharmacological activity make chalcones most suitable for study as anticancer agents. Hence, we now wish to report a series of chalcones synthesized from the above precursor. Molecular modelling and pharmacophore mapping of these chalcones with tubulin, investigation of their anticancer activity against A549 and HepG2 cell lines and a tubulin polymerization inhibition assay were carried out to test their biological efficacy. In addition, theoretical calculations were also performed by using DFT to elucidate the geometric and electronic properties of these new chalcones.

2. Results and discussion

2.1 Synthesis of chalcones

The chalcones were synthesized *via* a Claisen–Schmidt condensation reaction (Scheme 1) of *p*-[*N*,*N*-bis(2-chloroethyl)amino]-benzaldehyde (**1**) and various substituted acetophenones (**2a–f**). The structures of the resulting chalcones (**3a–f**) were confirmed by UV, IR, mass, ^1H and ^{13}C NMR spectral methods and single crystal X-ray diffraction studies.

2.2 Spectral measurements

2.2.1 Electronic spectra. The UV-visible absorption spectrum of the six compounds was recorded in the region around 200–800 nm using ethanol as a solvent. α,β-unsaturated carbonyl compounds usually show two absorption bands pertaining to the n–π* and π–π* transitions.[44] Chalcones show intense absorption peaks above 350 nm and weak bands at around 220–270 nm. All the compounds studied show two well defined absorption bands consistent with the above. **3a–c** show a strong absorption band between 380–402 nm while **3d–f** show a relatively weaker band at 400–430 nm which is due to n–π* transition in the conjugated chain including the carbonyl moiety. This λ_{max} value may be attributed to the molecule in its entirety and is not specific to a single chromophore. All six compounds show a weak absorption band at around 250–270 nm (π–π* transitions) due to the benzoyl or acrylophenone chromophore. Compounds **3a–c** and **3e** also

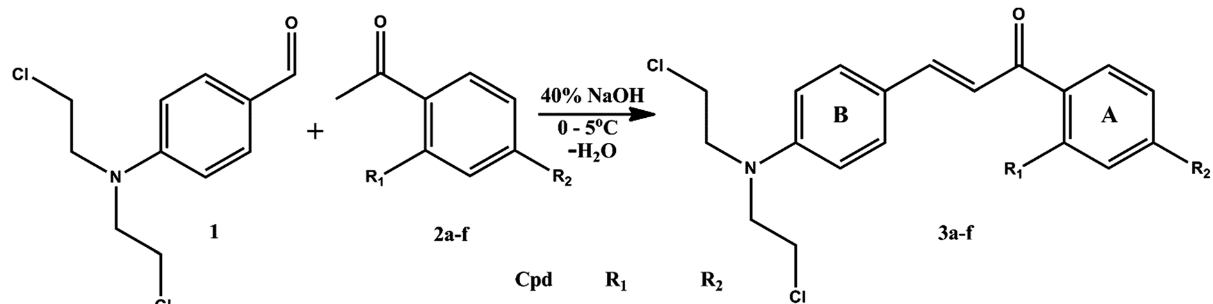

Cpd	R_1	R_2
3a	H	CH_3
3b	H	OCH_3
3c	OCH_3	OCH_3
3d	H	Br
3e	H	NO_2
3f	H	CH_2CH_3

Scheme 1 Synthesis of chalcones.

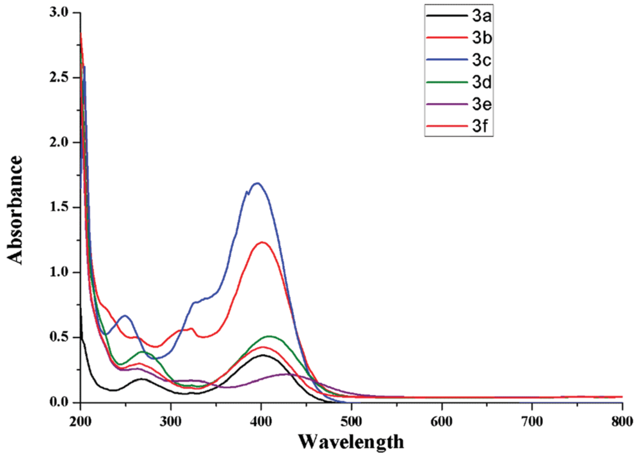

Fig. 1 UV absorption spectra of chalcones **3a–f**.

show a minor peak at around 320–340 nm (Fig. 1). Chalcones show bathochromic shifts if there are substituents other than hydrogen in the *para* position of rings A and B. Electron donating groups show a larger shift when they are present on ring B and no significant change when present on ring A. Ring B in all the compounds studied contains the same $-N(CH_2CH_2Cl)_2$ group. Since the literature reports that ring B is more sensitive to substitution than ring A,[45] significant changes in absorption were not expected. Electron withdrawing groups, however show a large bathochromic shift when present on ring A.[46] This is confirmed in **3d** and **3e** which show absorption bands at 410 nm and 428 nm due to the bromine and nitro group respectively. **3a** and **3f** show almost identical absorption bands, but **3a** shows greater intensity.

2.2.2 IR spectra. The IR spectra of all six compounds were studied. The stretching frequency of α,β-unsaturated carbonyl compounds usually lies in the range of 1660–1685 cm^{-1}. However, resonance with additional conjugation will lower the stretching frequency. The carbonyl stretching frequencies for all six compounds investigated occur at 1644–1647 cm^{-1} except for **3c** for which the carbonyl stretching frequency is located at 1596 cm^{-1}. This is probably due to the presence of two electron donating methoxy groups and intramolecular hydrogen bonding between the α-hydrogen and the methoxy oxygen. The C–Cl stretching frequency occurs at 520–869 cm^{-1} while aromatic C–N stretching is observed at 1246–1351 cm^{-1}. Absorption bands at 1435–1595 cm^{-1} are due to C=C stretching vibrations. Alkyl and aromatic C–H bending occur at 1335–1396 cm^{-1} and 807–817 cm^{-1} respectively. In compounds **3b** and **3c**, C–O stretching occurs at 1020–1347 cm^{-1}. Absorption bands at 1212–1252 cm^{-1} in these two compounds can be attributed to aromatic C–O stretching. The N–O symmetric and asymmetric stretching in **3e** occurs at 1351 and 1440–1513 cm^{-1}. The C–Br stretching in **3d** occurs at 528–661 cm^{-1}.

2.2.3 NMR spectra. The ^{1}H and ^{13}C NMR spectra were recorded for the synthesized compounds with d_6-DMSO as the solvent. The olefinic protons (7 and 8) appeared in the region of 7.59–7.81 ppm with different splitting patterns. In the case of **3a** and **3f** they appeared as singlets at 7.67 ppm. However, in the case of **3c**, the olefinic protons appeared as expected as two individual doublets at 7.31 and 7.45 ppm with the splitting constant of 15 Hz *ca.* For compounds **3b**, **3d** and **3e**, they appeared as multiplets and merged with the signals of other aromatic protons. In order to overcome ambiguity in the splitting of these protons, the ^{1}H NMR spectra were recorded in $CDCl_3$ to observe the splitting of olefinic protons. It was noted that the protons appeared as two doublets in the range of 7.75–7.80 ppm with the coupling constant of 15.4–15.7 Hz. This confirms that the olefinic protons are trans to each other. The reason for the appearance of a singlet may be due to complexation of a solute molecule with DMSO which leads to an anisotropic effect on the olefinic protons resulting in an anomalous change in the chemical shift.[47] The aromatic protons of both rings appear in the range of 6.70–8.20 ppm and are dependent on the various substituents present in both the rings. The methylene protons of the bis(chloroethyl)amino groups appear in the range of 3.65–3.83 ppm. In the ^{13}C spectrum, the carbonyl carbon appears between 188.20–190.60 ppm. The α and β vinylic carbon atoms give characteristic signals between 123.40–123.80 ppm and 142.60–146.90 ppm respectively. The assignment of individual protons and carbons is provided in Tables S1–S3 (ESI†).

2.3 X-ray crystallography

In order to understand the structural interactions between the molecules in a unit cell and their spatial arrangements, compounds **3a–f** were crystallized and diffracted at room temperature. The ORTEP diagram is presented in Fig. 2. Crystallographic data and unit cell dimensions are given in Table 1.

The molecules **3a–f**, except for **3c**, crystallized in a triclinic crystal system with a centrosymmetric space group $P\bar{1}$ and crystal **3c** crystallized in the monoclinic crystal system with a centrosymmetric space group *P*21/*c*. In the six compounds, the two aromatic rings A and B are connected through the backbone consisting of three carbon atoms (C7, C8 and C9) with the C=C bond length being an average of 1.40 Å and the dihedral angle of both the rings A and B being an average of ±18°. The dihedral angle between ring B and plane 3 falls between 15–21° corresponding to the *cisoid* conformation and that between ring A and plane 3 falls between 10–13° showing the presence of co-planarity in the molecules. This is also evident from DFT analysis (Fig. S2, ESI†). The olefinic double bond (C8–C9 ≈ 1.32 Å) is in the *E* configuration and is C_{sp^2} hybridized. The C10–C11 bond length of ring B is considerably higher than the normal value of 1.37 Å. This is attributed to the resonance character of ethyl amine (Fig. S2, ESI†). The bond length variations of the phenyl ring confirms that extended electronic conjugation is observed between the central –CH=CH–C(=O)– group and the bis(2-chloroethyl)amino benzene ring, which was further confirmed by the C(phenyl)–C(carbonyl) bond being considerably shorter (1.48 Å) than that in *p*-aminoacetophenone. In the crystal, the molecules are linked through intermolecular C–H···O and C–H···Cl hydrogen bonds, generating an edge fused ring motif (Fig. S1, ESI†). The hydrogen bond motifs are linked to each other to form a three dimensional network, which seems to be effective in the stabilization of the crystal

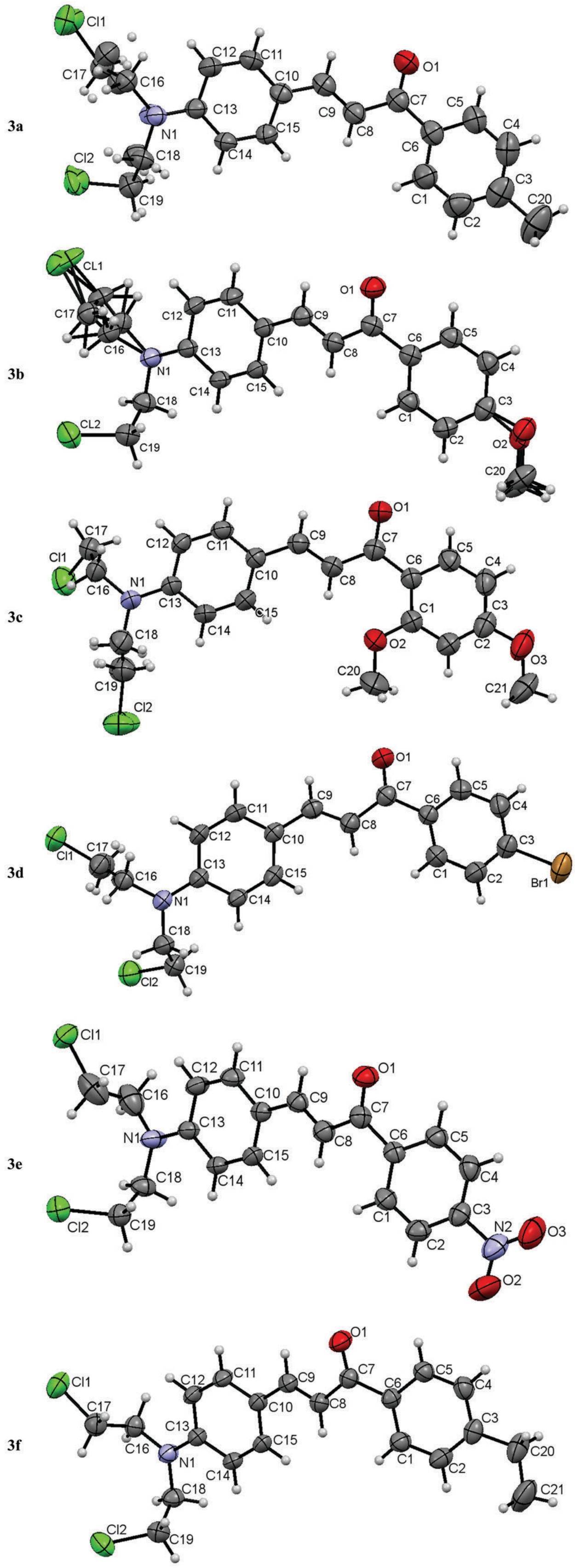

Fig. 2 ORTEP diagrams of the crystal structures of chalcones **3a–f**.

structure forming chains. The hydrogen bond lengths and angles are given in Table 2.

2.4 Computational study

2.4.1 Molecular docking. Molecular docking studies were performed to find the binding interactions of all six compounds with β-tubulin. Docking simulations showed that the ligands bind to the active site effectively. The ligand pose with the highest dock score was selected as the binding pose. The binding potential of the six compounds with tubulin was determined. The H-interactions, H-bond distance and binding energies were calculated. Docking simulations showed that ring A of compounds **3a–f** along with different substituents was buried deep in the hydrophobic site in β-tubulin surrounded by Valβ238, Cysβ241, Leuβ242, Leuβ248, Alaβ250, Leuβ252, Lysβ254, Leuβ255, Asnβ258, Alaβ316, Valβ318, Lysβ352 and Alaβ354. Similar results were observed when MDL 27048 and colchicine were also docked. The results obtained are in agreement with and further strengthened by what has been reported by Ducki *et al.*[48] Hence, these chalcones can be expected to react similarly to colchicine and podophyllotoxin in inhibiting cross-linking between Cysβ241 and Cysβ356.[49] Docking also showed that the chlorine atom of the [*N*,*N*-bis(2-chloroethyl)amino] group in chalcones **3a–b** and **d–f** was involved in hydrogen bonding with Lysβ352 with a D–H–A bond distance ranging from 3.35 to 3.55 Å. Out of the six chalcones docked, only **3c** was involved in hydrogen bonding with Lys β254 with a D–H–A bond distance of 3.39 Å. Since the behaviour of these chalcones is similar to that of colchicine, combretastastin, podophyllotoxin and MDL 27048, they can be considered to belong to the same pharmacophoric group and inhibit microtubule assembly effectively. All six ligands bound to tubulin more effectively than the well-known anti-mitotic agent MDL 27048 and precursor **1**. Compounds **3a**, **d** and **e** showed the best docking scores. Hence the compounds display a synergistic effect in the binding of tubulin due to the potential anticancer characteristics of the precursor **1**. Binding is seen to be stabilized by hydrogen bonding. The significant amino acid residues involved in the interaction were Lysβ352 and Lysβ254. All six compounds were bound to tubulin through the chlorine atoms attached to the *p*-[*N*,*N*-bis(2-chloroethyl) amino] group. The chlorine atoms serve as the acceptor to the donor amine of the amino acids Lysβ352 and Lysβ254. The binding mode of all six chalcones with β-tubulin is given in Fig. 3 and the H-interactions and docking score of MDL 27048, the precursor *p*-[*N*,*N*-bis(2-chloroethyl)amino]benzaldehyde and the chalcones are given in Table 3. Fig. S2 (ESI†) shows the consolidated binding model of the six chalcones, colchicine and MDL-27048 in the binding site of β-tubulin.

2.4.2 Pharmacophore mapping. Pharmacophore modelling of the six compounds was done using the HipHop model to identify various chemical features within the molecules that could be responsible for biological activity. Ten pharmacophore models were automatically generated and had alignment scores ranging from 16.20 to 16.25 (Table S4, ESI†). The best pharmacophore model was then selected and analysed. It had a six point pharmacophore denoted as RRHHHA (R – ring aromatic, H – hydrophobic group and A – hydrogen bond acceptor).

Table 1 Crystallographic data and unit cell dimensions of the chalcones **3a–f**

Identification code	3a	3b	3c	3d	3e	3f
CCDC	1042842	1061656	1035426	1402531	1426151	1426150
Chemical formula	$C_{20}H_{21}Cl_2NO$	$C_{20}H_{21}Cl_2NO_2$	$C_{21}H_{23}Cl_2NO_3$	$C_{19}H_{18}BrCl_2NO$	$C_{19}H_{18}Cl_2N_2O_3$	$C_{21}H_{23}Cl_2NO$
Formula weight	362.28	378.28	408.30	427.15	393.25	376.30
Temperature	293(2) K	293(2) K	293(2) K	296(2) K	296(2) K	296(2) K
Wavelength	0.71073 Å	0.71073 Å	0.71073 Å	0.71073 Å	0.71073 Å	0.71073 Å
Crystal size	0.350 × 0.350 × 0.300 mm	0.300 × 0.300 × 0.200 mm	0.350 × 0.300 × 0.300 mm	0.150 × 0.210 × 0.320 mm	0.140 × 0.220 × 0.250 mm	0.130 × 0.220 × 0.250 mm
Crystal habit	Clear, light yellow	Clear bright yellow	Clear light yellow	Clear light colourless rectangular	Clear light red rectangular	Clear light yellow block
Crystal system	Triclinic	Triclinic	Monoclinic	Triclinic	Triclinic	Triclinic
Space group	$P\bar{1}$	$P\bar{1}$	$P21/c$	$P\bar{1}$	$P\bar{1}$	$P\bar{1}$
Unit cell dimensions	a = 8.1897(4) Å^2 b = 9.3642(4) Å c = 12.3569(6) Å a = 77.9460(2)° b = 81.0530(2)° g = 83.0950(3)°	a = 8.3361(3) Å b = 9.1285(4) Å c = 12.2460(5) Å α = 81.630(2)° β = 84.5620(2)° γ = 83.1330(2)°	a = 14.8845(4) Å b = 16.7875(10) Å c = 8.0709(9) Å α = 90° β = 91.7080(3)° γ = 90°	a = 8.0990(2) Å b = 9.3548(2) Å c = 12.8639(4) Å α = 75.6264(12)° β = 79.1564(13)° γ = 79.0160(13)°	a = 8.0622(5) Å b = 9.3324(6) Å c = 12.5869(8) Å α = 78.3650(3)° β = 81.7410(4)° γ = 81.8320(4)°	a = 8.4268(3) Å b = 9.2446(3) Å c = 12.4656(4) Å α = 81.2037(13)° β = 85.3644(16)° γ = 84.7588(16)°
Volume	911.70(7) Å^3	912.49(6) Å^3	2015.80(3) Å^3	916.60(4) Å^3	911.68(10) Å^3	953.46(6) Å^3
Z	2	2	4	2	2	2
Density (calculated)	1.320 Mg m^{-3}	1.377 Mg m^{-3}	1.345 Mg m^{-3}	1.548 g cm^{-3}	1.433 g cm^{-3}	1.311 g cm^{-3}
Absorption coefficient	0.362 mm^{-1}	0.369 mm^{-1}	0.343 mm^{-1}	2.539 mm^{-1}	0.378 mm^{-1}	0.349 mm^{-1}
F(000)	380	396	856	432	408	396
θ range	2.233 to 24.999°	2.268 to 24.995°	2.43 to 25.000°	1.65 to 25.000°	1.66 to 24.990°	1.66 to 27.140°
Limiting indices	$-9 \leq h \leq 9$, $-11 \leq k \leq 11$, $-14 \leq l \leq 14$	$-9 \leq h \leq 9$, $-10 \leq k \leq 10$, $-14 \leq l \leq 14$	$-17 \leq h \leq 17$, $-19 \leq k \leq 19$, $-9 \leq l \leq 9$	$-9 \leq h \leq 9$, $-10 \leq k \leq 11$, $-15 \leq l \leq 15$	$-9 \leq h \leq 9$, $-11 \leq k \leq 11$, $-14 \leq l \leq 14$	$-10 \leq h \leq 10$, $-11 \leq \mathrm{k} \leq 11$, $-15 \leq l \leq 15$
Reflections collected/ unique (R_{int})	20979/3215 (0.0360)	23354/3209 (0.0279)	28756/3555 (0.0417)	13241/3231 (0.0185)	11309/	15022/4195 (0.0191)
Refinement method	Full-matrix least-squares on F^2	Full-matrix least-squares on F^2	Full-matrix least-squares on F^2	Full-matrix least-squares on F^2	Full-matrix least-squares on F^2	Full-matrix least-squares on F^2
Data/restraints/ parameters	3215/283/281	3209/131/269	3555/81/274	3231/0/237	11309/0/236	4195/0/227
Goodness-of-fit on F^2	1.064	0.872	1.063	1.033	1.065	1.057
Final R indices [$I > 2\sigma(I)$]	R_1 = 0.0428, wR_2 = 0.1058	R_1 = 0.0404, wR_2 = 0.1091	R_1 = 0.0458, wR_2 = 0.1094	R_1 = 0.0364, wR_2 = 0.0747	R_1 = 0.0640, wR_2 = 0.1984	R_1 = 0.0453, wR_2 = 0.1177
R indices (all data)	R_1 = 0.0757, wR_2 = 0.1319	R_1 = 0.0595, wR_2 = 0.1373	R_1 = 0.0922, wR_2 = 0.1472	R_1 = 0.0501, wR_2 = 0.0808	R_1 = 0.0792, wR_2 = 0.2187	R_1 = 0.0577, wR_2 = 0.1277
Largest diff. peak and hole	0.176 and −0.219 e Å^{-3}	0.242 and −0.273 e Å^{-3}	0.250 and −0.266 e Å^{-3}	0.466 and −0.559 e Å^{-3}	1.256 and −0.609 e Å^{-3}	d−0.409 e Å^{-3}

The compounds were then analysed based on the fit value. All the compounds had a fit value greater than 4 with similar pharmacophore features. Compound **3b** showed the best score of 5.76. Compound **3e**, which had the highest dock score had a fit value of 4.33. The two aromatic ring features are located in the two benzene rings. The three hydrophobic groups are the two chlorine atoms on ring B and the ring substituents in ring A. The H-bond acceptor is the α,β-unsaturated carbonyl moiety. Fig. S3 (ESI†) shows the pharmacophore model for the six chalcones generated by the HipHop model.

2.5 Biological activity

2.5.1 MTT (3-(4,5-dimethylthiazol-2-yl)-2,5-diphenyltetrazolium-bromide) assay. Compounds **3a–f** were tested for their anti-cancer effects against two different human cancer cell lines, A549 and HepG2, using an MTT (3-(4,5-dimethylthiazol-2-yl)-2,5-diphenyltetrazolium bromide) assay. All compounds exhibited significant activity with sub-micro molar IC_{50} values ranging from 0.089 to 0.200 μM. The low values of IC_{50} confirm that these chalcones are potent anticancer agents comparable to those already reported in the recent literature.[50–54] All the chalcones have a common *p*-[*N*,*N*-bis(2-chloroethyl)amino] group in ring B. Different substituents were appended to ring A in order to evaluate the structure–activity relationship of various chalcones towards the two cancer cell lines. The percentage cell viability against the two cancer cell lines is given in Fig. 4. The IC_{50} values are summarized in Table 4.

The introduction of methyl and nitro groups, as in **3a** and **3e**, at the *para* position in ring A showed the most potency in the activity of these compounds. This is well in keeping with the theoretical studies. Ethyl substituted chalcone showed the highest selectivity towards the human liver cancer cell line (HepG2) but the least activity towards human lung cancer cells (A549). Replacement of the methyl with the methoxy group however decreased the activity in both cell lines. However, two methoxy substituents at positions 2′ and 4′ showed high activity with A549 cells, but the least activity with HepG2 cells. Introduction of the bromine group, **3d**, lead to a decrease in the activity in both cell lines. Among the electron donating groups, it was found that the methyl group had the highest potency with the potency order being $CH_3 > C_2H_5 > OCH_3$. Although it is possible to draw a few conclusions from the above results,

Table 2 Hydrogen bond distances and angles for compounds **3a–f**

Cpd	D···H···A	d(D···H)	d(H···A)	d(D···A)	∠(DHA)
3a	C(17)–H(17A)···Cl2	0.97	2.86	3.70(5)	145.30
	C(19)–H(19A)···O1#1	0.97	2.66	3.37(6)	130.30
	C(16′)–H(16C)···Cl2′	0.97	2.63	3.36(2)	132.40
	C(17′)–H(17C)···O1#2	0.97	2.59	3.50(16)	156.50
	C(19′)–H(19D)···O1#3	0.97	2.50	3.40(3)	155.10
3b	C(19)–H(19A)···O1	0.97	2.69	3.63	162.87
	C(14)–H(14)···O1	0.93	2.76	3.67	166.20
	C(18)–H(18A)···O1	0.97	2.90	3.67	136.30
	C(19)–H(19B)···O1	0.97	2.93	3.60	126.60
3c	C(8)–H(8)···O(2)	0.93	2.18	2.77(4)	121.10
	C(18)–H(18B)···Cl1	0.97	2.88	3.48(5)	120.80
	C(20)–H(20B)···O3#4	0.96	2.65	3.53(5)	152.10
	C(17)–H(17B)···O1#5	0.97	2.53	3.30(4)	136.30
	C(18′)–H(18C)···Cl1#6	0.97	2.92	3.71(9)	138.50
3d	C(4)–H(4)···Cl1	0.93	2.94	3.76	147.40
	C(18)–H(18B)···O1	0.97	2.87	3.58	130.90
	C(19)–H(19B)···O1	0.97	2.70	3.42	131.29
	C(19)–H(19A)···O1	0.97	2.73	3.67	164.20
	C(14)–H(14)···O1	0.93	2.87	3.79	170.23
	C(16)–H(16A)···O1	0.97	2.96	3.90	168.43
3e	C(17)–H(17B)···Cl2	0.97	2.83	3.68	146.90
	C(12)–H(12)···O2	0.93	2.59	3.31	135.10
	C(16)–H(16B)···O3	0.97	2.46	3.34	151.60
	C(16)–H(16A)···O1	0.97	2.75	3.68	160.00
	C(19)–H(19B)···O1	0.97	2.79	3.50	130.30
3f	C(17)–H(17B)···Cl2	0.97	2.90	3.71	141.50
	C(16)–H(16B)···O1	0.97	2.69	3.62	161.60
	C(14)–H(14)···O1	0.93	2.73	3.64	167.70
	C(19)–H(19A)···O1	0.97	2.79	3.73	164.60
	C(18)–H(18A)···O1	0.97	2.78	3.46	127.50
	C(19)–H(19B)··· O1	0.97	2.78	3.53	135.00

Symmetry transformations used to generate equivalent atoms: #1 $x, y + 1, z$ #2 $-x + 1, -y, -z$ #3 $-x + 2, -y, -z$ #4 $-x + 2, y - 1/2, -z + 5/2$ #5 $-x + 1, y - 1/2, -z + 3/2$ #6 $x, -y - 1/2, z + 1/2$.

it must be noted that the literature reports many instances where the presence of electron donating groups have resulted in increased activity[55,56] while others have confirmed the reverse.[57,58] Hence, it can be concluded that the anticancer activity of the chalcones can be attributed not just to the type of substituent present in the rings, but more specifically to the size, position and stereochemistry of the substitution.

2.5.2 *In vitro* tubulin polymerization assay. Molecular docking studies showed that the six chalcones effectively bind to tubulin and inhibit the polymerization of α- and β-tubulin heterodimers into microtubules. Therefore, an *in vitro* tubulin inhibition polymerization assay was performed to test the extent of tubulin inhibition by the chalcones. The content of polymerized tubulin was monitored by measuring the absorbance at 340 nm every five minutes for half an hour (Fig. S4, ESI†). The results were then compared with the untreated control cells to evaluate the relative degree of change in optical density. It was found that all six compounds inhibited tubulin polymerization more effectively when compared to the positive control, thus confirming that the chalcones act as microtubule destabilizers. Among the six samples tested, **3e** was found to be the most potent. Molecular docking studies showed **3e** as one of the most effective in inhibiting tubulin, which is confirmed by the result obtained from the assay. It is evident that the presence of electron withdrawing groups greatly enhances tubulin inhibition. Among the electron donating groups, the ethyl group (**3f**) showed the greatest inhibition. The inhibition of **3a** was very effective and remained constant until the first 20 minutes, after which it increased rapidly. **3c** inhibited tubulin more effectively than **3b** reaffirming that the presence of methoxy groups increases tubulin inhibitory activity.[57] These results prove that the activity of chalcones is due to their inherent ability to bind to tubulin and inhibit its polymerization into microtubules.

2.6 Geometry optimization and frontier molecular orbitals

The optimized geometries of the six compounds are depicted in Fig. S5 (ESI†). Fig. S6 (ESI†) indicates the nature of delocalization for which C–C and C–N bond lengths fall between their respective single and double bond limits. The aromatic rings are connected through an olefin double bond. The π orbital from the C–C bond that connects two aromatic rings will have maximum overlap; as a result all the C–C bonds show partial double bond character. Hence, the C–C bond lengths in the chalcones fall in the range of 1.37–1.49 Å, which is shorter than a regular single bond.

To gain further insight into the excitation properties, the frontier molecular orbitals and band gaps of the newly synthesized chalcones were analysed. As observed in Fig. 6, the electron cloud distribution of the HOMO of all the compounds is mainly localized on the –CH=CH–C(=O)– group and the bis(2-chloroethyl)amino benzene ring B whereas the electron cloud distribution of the LUMO significantly lies over the CH=CH–C(=O)– group that is connected to the aromatic ring A and R_2 group. This clearly confirms that there is a presence of extensive delocalization between the donor and acceptor part of the molecule. The extent of the relative contribution of the LUMO varied slightly depending on the nature of the groups present in the R_2 group.

The frontier molecular orbital energy levels (HOMO−3 to LUMO+3) of the chalcones are shown in Fig. 5. All the chalcones show a narrow band gap ranging from 2.96 to 3.64 eV. The compound **3d** shows a lower band gap due to the presence of the nitro group in the R_2 position. The nitro group stabilizes the LUMO drastically as can be seen from the results observed. It can be seen in **3a–3c**, that the LUMO levels are destabilized by the R_2 group ($-CH_3$, $-OCH_3$, $-(OCH_3)_2$ respectively). As a result they have a maximum band gap of 3.59, 3.63 and 3.64 eV respectively. However, compounds **3d** and **3e** have a lower band gap (3.49 and 2.96 eV respectively) due to the presence of –Br and $-NO_2$ groups that stabilize the LUMO significantly. Overall, the HOMO lies in the range of −5.65 to −6.17 eV, whereas the LUMO falls in the range of −2.01 to −3.21 eV. The energy gaps of the compounds **3a–3f** are 3.59, 3.63, 3.64, 3.49, 2.96 and 3.60 eV, respectively.

To understand the nature of the various groups of the molecules and their individual contribution towards the HOMO and LUMO, % molecular orbital calculation was performed using QMForge software.[59] This gives the contribution of various fragments of the molecules towards their HOMO and LUMO.[60–63] The molecules

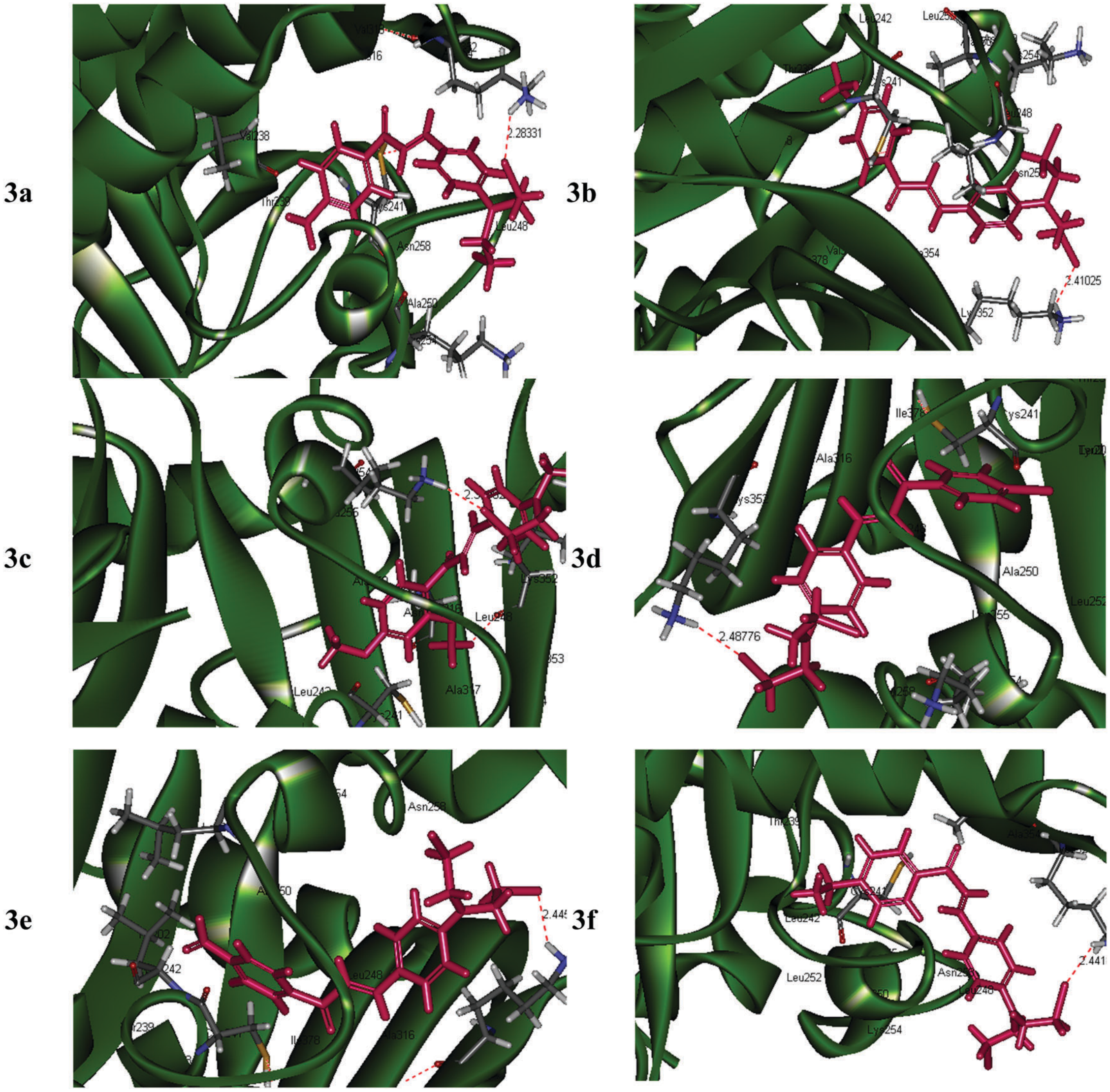

Fig. 3 Binding mode of chalcones **3a–f** within the colchicine site in β-tubulin. The chalcones are indicated as stick models and shown in pink. The active amino acid residues are shown as stick models.

Table 3 Docking score and hydrogen bond interactions of chalcones **3a–f**

Cpd	Dock score (kcal mol^{-1})	Lig score 1	Lig score 2	H-Interaction	H-Bond monitor	H-Bond distance	D···H···A angle	Binding energies	Fit value
MDL27048	45.03	2.31	4.32	LYS352	B:LYS352:HZ2 – Control_MDL.sdf:O22	1.75	134.34	−59.63	5.00
1	34.28	1.98	4.53	LYS254	B:LYS254:HZ3 – Cl-chalcones.cdx:Cl18	2.32	157.01	−73.43	2.34
3a	49.30	2.23	5.61	LYS352	B:LYS352:HZ2 – Cl-chalcones.cdx:Cl16	2.28	138.89	−41.40	5.38
3b	49.00	2.35	5.9	LYS352	B:LYS352:HZ2 – Cl-chalcones.cdx:Cl16	2.41	127.44	−66.19	5.76
3c	38.91	−999.90	−999.90	LYS254	B:LYS254:HZ1 – Cl-chalcones.cdx:Cl18	2.32	144.38	−80.78	4.73
3d	46.68	2.31	5.71	LYS352	B:LYS352:HZ2 – Cl-chalcones.cdx:Cl16	2.49	128.68	−68.21	5.62
3e	46.96	2.95	5.60	LYS352	B:LYS352:HZ2 – Cl-chalcones.cdx:Cl18	2.45	125.33	−49.26	4.33
3f	44.24	1.72	5.42	LYS352	B:LYS352:HZ2 – Cl-chalcones.cdx:Cl16	2.44	123.91	−51.07	5.36

are segmented into five fragments namely H-bond acceptor (–CH=CH–C(=O)– group), two aromatic rings (A and B), hydrophobic group (bis(2-chloroethyl)amino), R_1 (–OCH_3) and R_2 (–CH_3, –OCH_3, –OCH_3, –Br and NO_2) and their corresponding results are summarised in Table 5. For compounds **3a** and **3b**, the HOMO is equally contributed by the H-bond acceptor (42 and 40%) and aromatic ring (49 and 46%) with significant contribution from hydrophobic groups (8–14%). However, the HOMO of the compound **3c** is mainly contributed by two aromatic rings (60%) with significant contributions from hydrophobic (22%) and H-bond acceptor (18%) groups. The HOMOs of the compounds **3d–3f** are mainly from the H-bond acceptor and aromatic rings as observed in Fig. 6. In all the molecules, the LUMO is predominantly from the aromatic ring

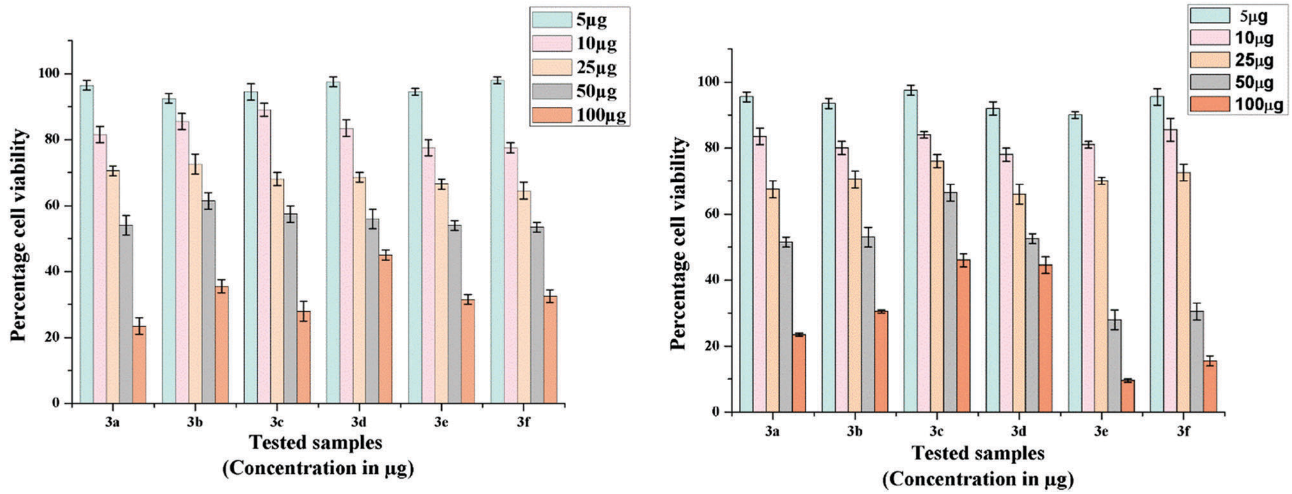

Fig. 4 Dose response graph of chalcones **3a–f** on A549 and HepG2 cells.

Table 4 IC_{50} values of all six chalcones against A549 and HepG2 cells

	IC_{50} (μM)	
Cpd	A549	HepG2
3a	0.161	0.156
3b	0.193	0.166
3c	0.153	0.198
3d	0.188	0.178
3e	0.160	0.091
3f	0.200	0.089

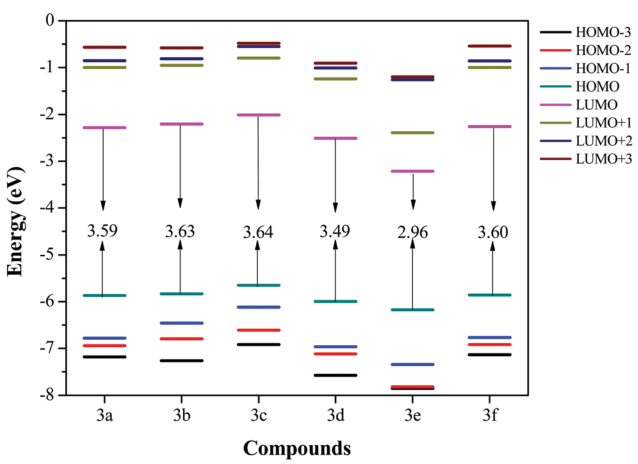

Fig. 5 Frontier molecular orbital energy levels of fluorophores computed at the B3LYP/6-311+G(d,p) level.

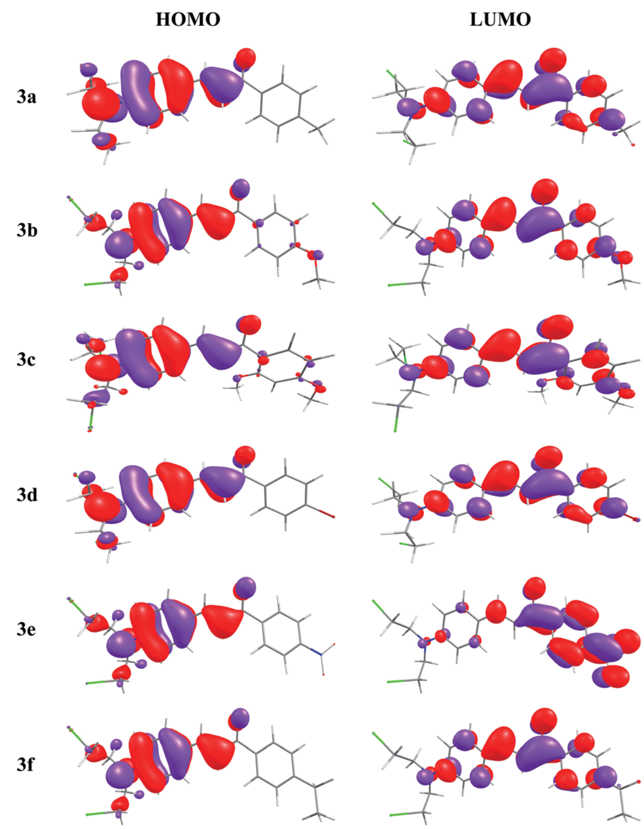

Fig. 6 Plots of the frontier molecular orbitals of the studied compounds computed at the B3LYP/6-311+G(d,p) level.

(over 58–72%) and 23–32% from the H-bond acceptor group with small contributions from the R_2 group. Hence it is understood that the HOMO can be further fine-tuned by engineering the aromatic group (B) and H-bond acceptor. In contrast, the LUMO can be lowered upon changing the aromatic ring (A) and R_2 group. This study sheds light on the relative significance and contributions of different moieties towards the electronic and optical behaviour of the chalcones.

2.7 Natural bond orbital analysis (NBO)

NBO analysis has been performed for the synthesized compounds at the B3LYP/6-311+G(d,p) level in order to elucidate the intramolecular, hybridization and charge transfer within the molecule. Several donor–acceptor interactions are observed for all the compounds and the importance of hyper conjugative interaction from the bonding to the antibonding orbital has been analysed. From second order perturbation energy analysis, it is found that

Table 5 Molecular orbital composition (%) of various fragments in the ground state geometry of compounds **3a–f**

	Compounds	H-Bond acceptor	Aromatic ring	Hydrophobic groups	R_1	R_2
HOMO	**3a**	41.73	48.94	8.97		0.36
	3b	40.28	45.45	14.05		0.23
	3c	17.45	59.61	22.26	0.36	0.33
	3d	41.75	49.91	8.30		0.05
	3e	35.57	56.12	8.29		0.03
	3f	46.57	41.19	1.86		10.38
LUMO	**3a**	22.82	71.88	3.55		1.75
	3b	25.83	67.71	6.15		0.32
	3c	28.47	64.75	5.88	0.52	0.39
	3d	28.12	69.45	2.32		0.11
	3e	21.92	71.12	1.12		5.84
	3f	31.80	57.66	5.88		4.66

3a

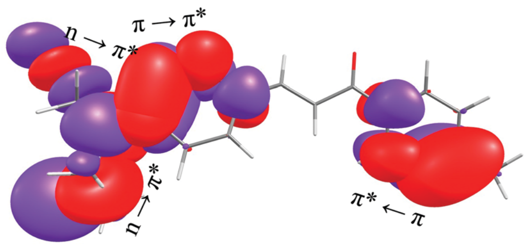

3e

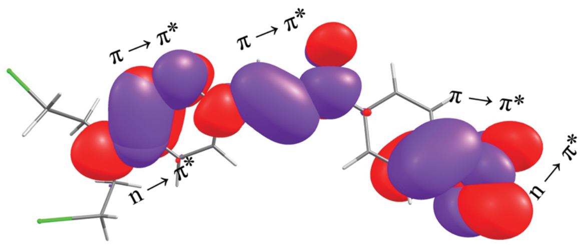

3f

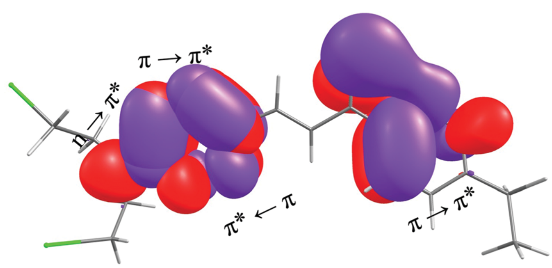

Fig. 7 Ground state stabilizing interactions of compounds **3a**, **3e** and **3f** showing $\pi \rightarrow \pi^*$ and $n \rightarrow \pi^*$ interactions.

$\pi \rightarrow \pi^*$ and $n \rightarrow \pi^*$ interactions are responsible for the ground state stabilization of all compounds (Fig. 7 and Fig. S7, ESI†). The $n \rightarrow \pi^*$ interactions arise from the lone pair on the oxygen or nitrogen to the π^* of the adjacent C–C bond. However, the $\pi \rightarrow \pi^*$ interaction arises entirely from the C–C bonds.

3. Experimental

3.1 Materials

All the chemicals and reagents used in the present work were of AnalaR grade and purchased from Sigma Aldrich. The precursor *p*-[*N*,*N*-bis(2-chloroethyl)amino]benzaldehyde was prepared according to the reported procedure.[38] The progress of the reaction and purity were monitored by TLC.

3.2 Measurements

Melting points were determined in open capillaries using Elico melting point apparatus. Thin layer chromatography was performed using silica gel G. UV-visible spectra of the compounds **3a–f** were studied using a Shimadzu UV-VIS spectrophotometer using ethanol as the solvent in the range of 200–800 nm. IR measurements were performed on a Shimadzu DR 8001 series FTIR instrument using KBr pellets. ^{1}H and ^{13}C NMR spectra were recorded with a BRUKER AV III 500 MHz FT NMR spectrometer with DMSO as the solvent at 500 MHz and 125 MHz respectively. Mass spectra were recorded using a Thermo Scientific Orbitrap Elite Mass spectrometer.

3.3 Unit cell determination

The X-ray diffraction study was carried out using a Bruker Axs kappa Apex II single crystal CCD diffractometer equipped with an Mo (Kα) (λ = 0.7107 Å) radiation source. The goniometer equipped to the diffractometer is a four circle goniometer with φ, χ, ω and 2θ axes by which the crystal is rotated. Six crystal specimens of size ranging from 0.13 × 0.22 × 0.25 mm to 0.35 × 0.35 × 0.30 mm were cut and mounted on a glass fiber using cyanoacrylate. The unit cell parameters were determined by collecting the diffracted intensities from 36 frames measured in three different crystallographic zones and using the method of difference vectors followed by data collection at 293 K using ω–φ scan modes.

3.4 Structure solution and refinement

The structures were solved using SHELXS 97,[64] revealing the positions of all non-hydrogen atoms. It was refined on F^2 by a full matrix least squares procedure using SHELXL 97. The non-hydrogen atoms were anisotropically refined and the H-atoms were allowed to ride over their parent atoms. The final cycle of refinement converged to their respective R_1 and wR_2 values (the individual values are given in Table 1) for the observed reflections. The maximum and minimum heights in the final difference Fourier map ranged from 0.176 to 1.256 and −0.219 to −0.609 e Å^{-3} respectively. PARST 97 was used to calculate least squares planes and asymmetry calculations. ORTEP and PLATON were used for the thermal ellipsoid plot and packing respectively.[65,66] PLATON was also used to create the non-bonded interacted graphics. The crystallographic data are shown in Table 1 and the bond distances and angles can be downloaded free of cost from the Cambridge Crystallographic Data website (www.ccdc.co.uk). The atomic coordinates and the respective isotropic displacement coefficients can be found in the deposited material. The CCDC number for each compound is given in Table 1.

3.5 Synthesis of chalcones

3.5.1 Synthesis of (*E*)-(4-bis(2-chloroethylamino)phenyl)-1-(*p*-tolyl)prop-2-en-1-one (3a). The precursor, *p*-[*N*,*N*-bis(2-chloroethyl)amino]benzaldehyde **1** (2 mmol), was dissolved in

25 mL of methanol and stirred with *p*-methyl acetophenone **2a** (2 mmol) in 10 mL of methanol in an ice bath. NaOH (40%, 2 mL) was then added dropwise to the mixture under ice-cold conditions. The reaction mixture was magnetically stirred for 24 hours. The progress was monitored by TLC until the reactants were completely consumed. The mixture was then poured into ice and the yellow solid precipitate obtained was filtered, washed with water, dried and recrystallized from 1:1 methanol and dichloromethane to give light yellow crystals of the chalcone **3a**. Yield: 87%, m.p.: 108 °C. Anal. calcd for $C_{20}H_{21}Cl_2NO$: C, 66.30; H, 5.84; N, 3.87. Found: C, 66.32; H, 5.82; N, 3.84%. λ_{max} (ethanol): 268, 324, 402 nm (37313.43, 30864.20, 24875.62 cm^{-1}). FT-IR (ν_{max}, cm^{-1}) in KBr = 1644.50 (α,β-unsaturated C=O), 596–869 (C–Cl), 1246–1346 (C–N). ^{1}H NMR δ_H (500 MHz; DMSO-d$_6$; TMS) 2.36–2.44 (3H, m, H-1), 3.75–3.87 (8H, m, H-14, 14′, 13, 13′), 6.81–6.85 (2H, m, $J_{11',11,10',10}$ = 8.5 Hz, H-11′, 11), 7.36 (2H, d, J = 7.9 Hz, H-3, 3′), 7.67 (2H, s, H-7, 8), 7.70–7.76 (2H, m, $J_{10',10,11',11}$ = 8.5 Hz, H-10′, 10), 8.01–8.05 (2H, m, J = 7.9 Hz, H-4, 4′). ^{1}H NMR δ_H (500 MHz; CDCl$_3$; TMS) 2.43 (3H, s, H-1), 3.62–3.70 (4H, m, H-14, 14′), 3.75–3.85 (4H, m, H-13, 13′), 6.70 (2H, d, $J_{11',11,10',10}$ = 7.9 Hz, H-11′, 11), 7.29 (2H, d, J = 7.9 Hz, H-3, 3′), 7.36 (1H, d, J = 15.6 Hz, H-7), 7.50–7.62 (2H, m, H-10′, 10), 7.75 (1H, d, J = 15.6 Hz, H-8), 7.92 (2H, d, J = 7.6 Hz, H-4, 4′). ^{13}C NMR δ_C (126 MHz; DMSO-d$_6$) 21.14 (C-1), 41.05 (C-14, 14′), 51.76 (C-13, 13′), 111.88 (C-11′, 11), 117.04 (C-7), 123.21 (C-9), 128.38 (C-3, 3′), 129.23 (C-4, 4′), 130.93 (C-10′, 10), 135.64 (C-5), 142.93 (C-2), 144.27 (C-8), 148.61 (C-12), 188.24 (C-6). ESI-MS: *m*/*z* 362.1064 [M]$^+$, calculated 362.1073.

The method described above was followed for the synthesis of all the chalcones.

3.5.2 Synthesis of (*E*)-(4-bis(2-chloroethylamino)phenyl)-1-(4-methoxyphenyl)prop-2-en-1-one (3b). Chalcone **3b** was synthesized from aldehyde **1** and *p*-methoxy acetophenone **2b**. The yellow solid obtained was filtered, washed, dried and recrystallized from 1:1 methanol and dichloromethane to give bright yellow crystals. Yield 78%, m.p.: 109 °C. Anal. calcd for $C_{20}H_{21}Cl_2NO_2$: C, 63.50; H, 5.60; N, 3.70. Found: C, 63.48; H, 5.61; N, 3.73%. λ_{max} (ethanol): 260, 322, 400 nm (38461.54, 31055.90, 25000.00 cm^{-1}). FT-IR (ν_{max}, cm^{-1}) in KBr = 1646 (α,β-unsaturated C=O), 600–869 (C–Cl), 1252–1347 (C–N), 1021–1347 (C–O). ^{1}H NMR δ_H (500 MHz; DMSO-d$_6$; TMS) 3.75–3.85 (8H, m, H-14, 14′, 13, 13′), 3.86 (3H, s, H-1′), 6.83 (2H, br d, J = 8.8 Hz, H-11′, 11), 7.07 (2H, d, J = 8.8 Hz, H-3, 3′), 7.67 (2H, d, J = 7.6 Hz, H-8), 7.73 (2H, br d, J = 8.8 Hz, H-10′, 10), 8.13 (2H, d, J = 8.8 Hz, H-4, 4′). ^{1}H NMR δ_H (500 MHz; CDCl$_3$; TMS) 3.69 (4H, t, J = 6.9 Hz, H-14, 14′), 3.83 (4H, t, J = 7.0 Hz, H-13, 13′), 3.91 (3H, s, H-1′), 6.73 (2H, d, J = 8.9 Hz, H-11′, 11), 7.00 (2H, d, $J_{3,3',10',10}$ = 8.9 Hz, H-3, 3′), 7.40 (1H, d, J = 15.4 Hz, H-7), 7.59 (2H, d, $J_{10',10,3,3'}$ = 8.7 Hz, H-10′, 10), 7.78 (1H, d, J = 15.4 Hz, H-8), 8.05 (2H, d, J = 8.7 Hz, H-4, 4′). ^{13}C NMR δ_C (126 MHz; DMSO-d$_6$) 41.5 (C-14, 14′), 52.3 (C-13, 13′), 56.0 (C-1′), 112.4 (C-3, 3′), 114.4 (C-11′, 11), 117.5 (C-7), 123.8 (C-9), 131.0 (C-10′, 10), 131.3 (C-4, 4′), 131.5 (C-5), 144.2 (C-8), 149.0 (C-12), 163.3 (C-2), 187.6 (C-6). ESI-MS: *m*/*z* 378.1017 [M]$^+$, calculated 378.1022.

3.5.3 Synthesis of (*E*)-(4-bis(2-chloroethylamino)phenyl)-1-(2,4-dimethoxyphenyl)prop-2-en-1-one (3c). Chalcone **3c** was synthesized from aldehyde **1** and 2,4-dimethoxy acetophenone **2c**. The yellow solid obtained was filtered, washed, dried and recrystallized from methanol to give bright yellow crystals. Yield 76%, m.p.: 86 °C. Anal. calcd for $C_{21}H_{23}Cl_2NO_3$: C, 61.77; H, 5.68; N, 3.43. Found: C, 61.76; H, 5.65; N, 3.45%. λ_{max} (ethanol): 204, 250, 338, 384, 396 nm (49019.61, 40000.00, 29585.80, 26041.67, 25252.53 cm^{-1}). FT-IR (ν_{max}, cm^{-1}) in KBr = 1596 (α,β-unsaturated C=O), 541–811 (C–Cl), 1250–1335 (C–N), 1020–1335 (C–O). ^{1}H NMR δ_H (500 MHz; DMSO-d$_6$; TMS) 3.75–3.82 (8H, m, H-13, 14, 13′, 14′), 3.85 (3H, s, H-1′), 3.89 (3H, s, H-15), 6.63 (1H, d, J = 8.5 Hz, H-3), 6.68 (1H, s, H-3′), 6.81 (2H, d, J = 8.6 Hz, H-11, 11′), 7.31 (1H, d, J = 15.7 Hz, H-7), 7.47 (1H, d, J = 15.7 Hz, H-8), 7.53–7.61 (3H, m, H-4, 10, 10′), 7.71–7.73 (1H, d, J = 8.4 Hz, H-4). ^{1}H NMR δ_H (500 MHz; CDCl$_3$; TMS) 3.65 (4H, t, J = 6.9 Hz, H-14, 14′), 3.78 (4H, t, J = 7.0 Hz, H-13, 13′), 3.87 (3H, s, H-1′), 3.89 (3H, s, H-15), 6.50 (1H, d, J = 2.1 Hz, H-3′), 6.56 (1H, dd, J = 8.6 Hz, J = 2.2 Hz, H-3), 6.68 (2H, d, J = 8.9 Hz, H-11′, 11), 7.33 (1H, d, J = 15.7 Hz, H-7), 7.51 (2H, d, J = 8.7 Hz, H-10′, 10), 7.61 (1H, d, J = 15.7 Hz, H-8), 7.70–7.74 (1H, m, H-4). ^{13}C NMR δ_C (126 MHz; DMSO-d$_6$) 41.47 (C-14, 14′), 52.28 (C-13, 13′), 56.01 (C-1′), 56.33 (C-19), 99.11 (C-3′), 106.25 (C-3), 112.45 (C-11′, 11), 122.47 (C-5), 122.99 (C-7), 123.77 (C-9), 130.82 (C-10′, 10), 142.59 (C-8), 148.77 (C-12), 160.31 (C-2), 163.94 (C-4′), 189.78 (C-6) ESI-MS: *m*/*z* 408.1123 [M]$^+$, calculated 408.1128.

3.5.4 Synthesis of (*E*)-(4-bis(2-chloroethylamino)phenyl)-1-(4-bromophenyl)prop-2-en-1-one (3d). Chalcone **3d** was synthesized from aldehyde **1** and *p*-bromo acetophenone **2d**. The yellow solid obtained was filtered, washed, dried and recrystallized from 1:1 methanol and dichloromethane to give colourless crystals. Yield 71%, m.p.: 138 °C. Anal. calcd for $C_{19}H_{18}BrCl_2NO$: C, 53.42; H, 4.25; N, 3.28. Found: C, 53.44; H, 4.23; N, 3.25%. λ_{max} (ethanol): 268, 410 nm (37313.43, 24390.24 cm^{-1}). FT-IR (ν_{max}, cm^{-1}) in KBr = 1644 (α,β-unsaturated C=O), 661–808 (C–Cl), 1248–1346 (C–N), 528–661 (C–Br). ^{1}H NMR δ_H (500 MHz; DMSO-d$_6$; TMS) 3.71–3.89 (8H, m, H-14, 14′, 13, 13′), 6.83 (2H, br d, J = 8.5 Hz, H-11′, 11), 7.59–7.80 (6H, m, H-7, 8, 10′, 10, 3, 3′), 8.05 (2H, br d, J = 8.2 Hz, H-4, 4′). ^{13}C NMR δ_C (126 MHz; DMSO-d$_6$) 41.54 (C-14, 14′), 52.24 (C-13, 13′), 112.39 (C-11′, 11), 117.06 (C-7), 123.55 (C-9), 127.16 (C-2), 130.77 (C-10′, 10), 131.66 (C-3, 3′), 132.18 (C-4, 4′), 137.68 (C-5), 145.72 (C-8), 149.34 (C-12), 188.28 (C-6). ESI-MS: *m*/*z* 426.0027 [M]$^+$, calculated 426.0022.

3.5.5 Synthesis of (*E*)-(4-bis(2-chloroethylamino)phenyl)-1-(4-nitrophenyl)prop-2-en-1-one (3e). Chalcone **3e** was synthesized from aldehyde **1** and *p*-nitro acetophenone **2e**. The red solid obtained was filtered, washed, dried and recrystallized from acetone to give light red crystals. Yield 91%, m.p.: 185 °C. Anal. calcd for $C_{19}H_{18}Cl_2N_2O_3$: C, 58.03; H, 4.61; N, 7.12. Found: C, 58.06; H, 4.63; N, 7.15%. λ_{max} (ethanol): 264, 322, 428 nm (37878.79, 31055.90, 23364.49 cm^{-1}). FT-IR (ν_{max}, cm^{-1}) in KBr = 1645.70 (α,β-unsaturated C=O), 531–846 (C–Cl), 1251–1351 (C–N), 1351 (NO symmetric), 1440–1513 (NO asymmetric). ^{1}H NMR δ_H (500 MHz; DMSO-d$_6$; TMS) 3.75–3.81 (4H, m, H-14, 14′), 3.82–3.88 (4H, m, H-13, 13′), 6.86 (2H, d, J = 8.7 Hz, H-11′, 11), 7.63–7.81 (4H, m, H-7, 8, 10′, 10), 8.27–8.43 (4H, m, H-4, 4′, 3, 3′). ^{1}H NMR δ_H (500 MHz, CDCl$_3$; TMS) 3.69 (4H, t, J = 7.0, H-14, 14′), 3.84 (4H, t, J = 7.0, H-13, 13′), 6.74 (2H, d, J = 9.0 Hz, H-11′, 11), 7.31 (1H, d, J = 15.6 Hz, H-7), 7.60 (2H, d, J = 8.9 Hz, H-10′, 10), 7.81 (1H, d, J = 15.6 Hz, H-8), 8.13 (2H, d,

$J = 9.0$ Hz, H-3, 3′), 8.36 (2H, d, $J = 8.5$ Hz, H-4, 4′). ^{13}C NMR δ_C (126 MHz; DMSO-d_6) 41.54 (C-14, 14′), 52.20 (C-13, 13′), 112.44 (C-11′, 11), 117.17 (C-7), 123.37 (C-9), 124.27 (C-3, 3′), 130.05 (C-10′, 10), 131.94 (C-4, 4′), 143.69 (C-5), 146.87 (C-8), 149.67 (C-12), 150.01 (C-2), 188.24 (C-6). ESI-MS: m/z 393.0764 $[M]^+$, calculated 393.0767.

3.5.6 Synthesis of (*E*)-(4-bis(2-chloroethylamino)phenyl)-1-(4-ethylphenyl)prop-2-en-1-one (3f). Chalcone **3f** was synthesized from aldehyde **1** and *p*-ethyl acetophenone **2f**. The yellow solid obtained was filtered, washed, dried and recrystallized from 1 : 1 methanol and dichloromethane to give light yellow crystals. Yield 63%, m.p.: 96 °C. Anal. calcd for $C_{21}H_{23}Cl_2NO$: C, 67.02; H, 6.16; N, 3.72. Found: C, 67.01; H, 6.14; N, 3.70%. λ_{max} (ethanol): 266, 402 nm (37593.98, 24875.62 cm^{-1}). FT-IR (ν_{max}, cm^{-1}) in KBr = 1644.70 (α,β-unsaturated C═O), 528–868 (C–Cl), 1245–1347 (C–N). ^{1}H NMR δ_H (500 MHz; DMSO-d_6; TMS) 1.22 (3H, br t, $J = 7.6$ Hz, H-1′), 2.69 (2H, q, $J = 7.3$ Hz, H-1), 3.69–3.92 (8H, m, H-14, 14′, 13, 13′), 6.83 (2H, br d, $J = 8.2$ Hz, H-11′, 11), 7.38 (2H, br d, $J = 7.6$ Hz, H-3, 3′), 7.67 (2H, s, H-7, 8), 7.73 (2H, br d, $J = 8.5$ Hz, H-10′, 10), 8.05 (2H, br d, $J = 7.6$ Hz, H-4, 4′). ^{1}H NMR δ_H (500 MHz, $CDCl_3$; TMS) 1.30 (3H, t, $J = 7.6$ Hz, H-1′), 2.75 (2H, q, $J = 7.6$ Hz, H-1), 3.69 (4H, t, $J = 6.9$ Hz, H-14, 14′), 3.82 (4H, t, $J = 6.9$ Hz, H-13, 13′), 6.72 (2H, d, $J = 8.9$ Hz, H-11′, 11), 7.34 (2H, d, $J = 8.4$ Hz, H-3, 3′), 7.39 (1H, d, $J = 15.4$ Hz, H-7), 7.59 (2H, d, $J = 8.7$ Hz, H-10′, 10), 7.78 (1H, d, $J = 15.6$ Hz, H-8), 7.97 (2H, d, $J = 8.2$ Hz, H-4, 4′). ^{13}C NMR δ_C (126 MHz; DMSO-d_6) 15.70 (C-1′), 28.66 (C-1), 41.52 (C-14, 14′), 52.26 (C-13, 13′), 112.37 (C-11′, 11), 117.58 (C-7), 123.71 (C-9), 128.52 (C-3, 3′), 128.95 (C-4, 4′), 131.41 (C-10′, 10), 136.42 (C-5), 144.74 (C-8), 149.08 (C-12), 149.47 (C-2), 188.79 (C-6). ESI-MS: m/z 376.1227 $[M]^+$, calculated 376.1229.

3.6 Computational study

3.6.1 Molecular modelling. Development of computational methods for lead generation and optimization are important for the drug discovery process.[67] In this study, an integration of docking studies and pharmacophore modelling has been applied in order to identify compounds that contain important chemical features and bind at the active site of the protein receptor. The potency of the synthesized compounds was investigated by studying their interaction with β-tubulin. The 3D crystal structure of the colchicine site of tubulin (PDB ID: 3E22) was downloaded from the RCSB Protein Data Bank website (www.rcsb.org/pdb) and used. Ligands and water molecules were removed from the binding sites. Docking studies were performed with Discovery Studio (Accelrys) by simulation of all six compounds into the colchicine binding site of β-tubulin. All docking and pharmacophore studies were run using the Ligand-Fit dock protocol of Discovery Studio program. The compounds along with colchicine and MDL-27048 were docked into the colchicine binding pocket at the interface of α- and β-tubulin. All six compounds synthesized obey Lipinski's rule of five[68] and hence could be potential drug candidates.

All calculations on the synthesized compounds have been performed using Gaussian 09 code.[69] The ground-state geometries of the molecules were fully optimized at the DFT level using the B3LYP[70–73] functional with the 6-311+G(d,p) basis set. The vibrational frequency analysis of the optimized geometries confirms that all the optimized geometries correspond to minima on the potential energy surface by exhibiting all real frequencies. Natural bond orbital (NBO) analysis[74] has been performed at the B3LYP/6-311+G(d,p) level in order to elucidate the intramolecular charge transfer within the molecules. The second order perturbation energy analysis was carried out to evaluate the donor–acceptor interactions in the ground state of the molecules.

3.6.2 Pharmacophore mapping. Pharmacophore modelling studies were also performed to understand the key interactions in ligand binding. Due to the efficiency in virtual screening, the pharmacophore model method is an important tool in drug discovery.[75] Common feature pharmacophore generation which is a ligand-based approach using the HipHop model was used. The pharmacophoric features selected for creating sites were H-bond acceptor (A), H-bond donor (D), hydrophobic group (H) and aromatic ring (R). A maximum of 1119 conformations were generated with an average of 186 conformations per molecule and an energy threshold of 20 kcal mol^{-1}. The conformers were generated using the 'Generate conformations' protocol by the FAST conformation method. Ten pharmacophore models were generated and the best one based on the rank and descriptor set was selected.

3.7 Biological activity

3.7.1 MTT (3-(4,5-dimethylthiazol-2-yl)-2,5-diphenyltetrazoliumbromide) assay. The effect of the six chalcones on human liver (hepatocellular carcinoma) cancer cells (HepG2) and human lung cancer cells (A549) was determined using the MTT cell viability assay. The cells and test compounds dissolved in DMSO were prepared in 96-well plates containing a final volume of 100 μL per well. They were maintained at 37 °C in a humidified incubator with 5% CO_2 and 95% air. The medium was changed twice weekly and regularly examined. 10 μL MTT solution was added to the cells to achieve a final concentration of 0.45 mg mL^{-1} and incubated. The purple formazan crystals formed were dissolved in DMSO and the absorbance was recorded at 570 nm. Six repetitions were performed for each concentration. The inhibition percentages of the compounds were assessed and the IC_{50} values were calculated from concentration-response curves by regression analysis.

3.7.2 *In vitro* tubulin polymerization assay. The effect of the six chalcones was determined by *in vitro* tubulin inhibition assay using a commercial tubulin polymerization assay kit (porcine tubulin and fluorescence based), Cytoskeleton Inc. The procedure was carried out according to the manufacturer's protocol. Purified tubulin (4 mg mL^{-1}) in G-PEM buffer (80 mM PIPES pH 6.9, 2 mM $MgCl_2$ and 0.5 mM EGTA plus 1 mM GTP) was incubated with the mean IC_{50} concentration of the compounds in pre-warmed plates. Tubulin polymerization was analysed based on a time dependent increase in fluorescence during polymerization. Fluorescence changes were recorded at 340 nm by placing the plates into a spectrophotometer at 37 °C at 5 minute intervals. Six repetitions were done for each compound.

4. Conclusion

Structure based molecular docking studies were performed *in silico* to study the binding mode of a series of six chalcones with a β-tubulin crystal structure (3E22) downloaded from the PDB website. The chalcones were found to occupy the hydrophobic colchicine binding site surrounded by key amino acid residues such as Cysβ241, Leuβ242, Lysβ254, Alaβ316, Lysβ352, Alaβ354, *etc.* The orientation of the chalcones in the binding site is similar to that of colchicine. The orientations are stabilized by hydrogen bonding and van der Waals interactions. Docking studies showed that the six compounds bind more effectively to β-tubulin than the well-known anti-mitotic agent MDL 27048 or the precursor **1**. Pharmacophore mapping was also done generating a six point pharmacophore with an alignment score ranging from 16.20 to 16.25. The chalcones were then synthesized using *p*-[*N*,*N*-bis(2-chloroethyl)amino]benzaldehyde and substituted acetophenones *via* the Claisen–Schmidt condensation reaction. Their structures were characterized by spectroscopic techniques and their crystal structure was determined by the single crystal XRD method. Compounds **3a–b** and **d–f** crystallized in the triclinic system with a centrosymmetric space group $P\bar{1}$ and crystal **3c** crystallized in the monoclinic crystal system with a centrosymmetric space group *P*21/*c*. The molecules are linked through intermolecular C–H···O and C–H···Cl hydrogen bonds, generating the edge fused ring motif. The DFT results show that the HOMO of all chalcones lies in the range of −5.65 to −6.17 eV and the LUMO falls in the range of −2.01 to −3.21 eV. The results of molecular analysis reveal that the HOMO can be fine-tuned further by engineering the aromatic group (B) and H-bond acceptor and the LUMO can be lowered upon changing the aromatic ring (A) and R_2 group. NBO analysis reveals that the ground states of all the compounds are mainly stabilized by $\pi \rightarrow \pi^*$ and $n \rightarrow \pi^*$ interactions. The chalcones were evaluated for their anticancer activity against A549 and HepG2 cancer cells. They exhibited very high activity giving IC_{50} values ranging from 0.153 to 0.200 μM against A549 cells and 0.089 to 0.198 μM against HepG2 cells. They were also tested for their inhibition of tubulin assembly at the mean IC_{50} concentration using an *in vitro* tubulin polymerization inhibition assay. Of the six compounds tested, **3e** showed the highest inhibition against both the cancer cell lines and tubulin. These results correlate well with the theoretical studies performed. Therefore, it may be concluded that *p*-[*N*,*N*-bis(2-chloroethyl)amino]benzaldehyde substituted chalcone derivatives show a synergistic effect towards controlling cancer cell lines and tubulin polymerization. Furthermore, the present MDL-27048 binding model and the proposed pharmacophores along with the DFT study reports will provide useful guidelines for the future design of new chemical entities of microtubule targeted anticancer agents.

Acknowledgements

The authors thank the management of Sathyabama University for their kind support and encouragement during the course of the above work and SAIF, IIT Madras for the spectral measurements.

References

1 R. Romagnoli, P. G. Baraldi, M. D. Carrion, C. L. Cara, O. Cruz-Lopez, M. Tolomeo, S. Grimaudo, A. Di Cristina, N. Zonta, M. Pipitone, J. Balzarini, A. Brancale and E. Hamel, *Bioorg. Med. Chem.*, 2009, **17**, 6862–6871.
2 R. Romagnoli, P. G. Baraldi, M. D. Carrion, O. Cruz-Lopez, M. Tolomeo, S. Grimaudo, A. Di Cristina, M. R. Pipitone, J. Balzarini, A. Brancale and E. Hamel, *Bioorg. Med. Chem.*, 2010, **18**, 5114–5122.
3 E. Nogales, *Annu. Rev. Biophys. Biomol. Struct.*, 2001, **30**, 397–420.
4 M. A. Jordan and L. Wilson, *Nat. Rev. Cancer*, 2004, **4**, 253–265.
5 L. Hu, Z. R. Li, Y. Li, J. Qu, Y. H. Ling, J. D. Jiang and D. W. Boykin, *J. Med. Chem.*, 2006, **49**, 6273–6282.
6 D. E. Pryor, A. O'Brate, G. Bilcer, J. F. Diaz, Y. Wang, M. Kabaki, M. K. Jung, J. M. Andreu, A. K. Ghosh, P. Giannakakou and E. Hamel, *Biochemistry*, 2002, **41**, 9109–9115.
7 S. Sengupta and S. A. Thomas, *Expert Rev. Anticancer Ther.*, 2006, **6**, 1433–1447.
8 J. A. Hadfield, S. Ducki, N. Hirst and A. T. McGown, *Prog. Cell Cycle Res.*, 2003, **5**, 309–325.
9 S. Ducki, G. Mackenzie, N. J. Lawrence and J. P. Snyder, *J. Med. Chem.*, 2005, **48**(2), 457–465.
10 J. Lowe, H. L. Li, K. H. Downing and E. Nogales, *J. Mol. Biol.*, 2001, **313**(5), 1045–1057.
11 R. C. Weisenberg, G. G. Borisy and E. W. Taylor, *Biochemistry*, 1968, **7**, 4466–4479.
12 S. Uppuluri, L. Knipling, D. L. Sackett and J. Wolff, *Proc. Natl. Acad. Sci. U. S. A.*, 1993, **90**, 11598–11602.
13 M. Schmidt and H. Bastians, *Drug Resist. Updates*, 2007, **10**, 162–181.
14 C. Dumontet and B. I. Sikic, *J. Clin. Oncol.*, 1999, **17**, 1061–1070.
15 N. K. Sahu, S. S. Balbhadra, J. Choudhary and D. V. Kohli, *Curr. Med. Chem.*, 2012, **19**, 209–225.
16 J. S. Park, D. H. Kim, J. K. Lee, D. H. Kim, H. K. Kim, H. J. Lee and H. C. Kim, *Bioorg. Med. Chem. Lett.*, 2010, **20**, 1162–1164.
17 P. M. Sivakumar, T. Muthu Kumar and M. Boble, *Chem. Biol. Drug Des.*, 2009, **74**, 68–79.
18 D. Alwani Zainuri, S. Arshad, N. Che Khalib, I. Abdul Razak, R. R. Pillai, S. Fariza Sulaiman, N. Shafiqah Hashim, K. Leong Ooi, S. Armakovic, S. J. Armakovic, C. Y. Panicker and C. Van Alsenoy, *J. Mol. Struct.*, 2017, **1128**, 520–533.
19 M. Liu, P. Wilairat and M. L. Go, *J. Med. Chem.*, 2001, **44**, 4443–4452.
20 J. N. Dominguez, C. Leon, J. Rodrigues, N. Gamboa de Dominguez, J. Gut and P. J. Rosenthal, *J. Med. Chem.*, 2005, **48**, 3654–3658.
21 Y. M. Lin, Y. Zhou, M. T. Flavin, I. M. Zhou, W. Nie and F. C. Chen, *Bioorg. Med. Chem.*, 2002, **10**, 2795–2802.
22 H. Rücker, N. Al-Rifai, A. Rascle, E. Gottfried, L. Brodziak-Jarosz, C. Gerhäuser, T. P. Dick and S. Amslinger, *Org. Biomol. Chem.*, 2015, **13**, 3040–3047.
23 D. K. Mahapatra, V. Asati and S. K. Bharti, *Eur. J. Med. Chem.*, 2015, **92**, 839–865.
24 H. Qin, Z. Shang, I. Jantan, O. U. Tan, M. A. Hussain, M. Sherd and S. N. Abbas Bukhari, *RSC Adv.*, 2015, **5**, 46330–46338.

25 L. Wanga, Y. W. Y. Tian, J. Shang, X. Sun, H. Chen, H. Wang and W. Tan, *Bioorg. Med. Chem.*, 2017, **25**, 360–371.
26 M. L. Edwards, D. M. Stemerick and P. S. Sunkara, *J. Med. Chem.*, 1990, **33**, 1948–1954.
27 Y. N. Shen, L. Lin, H. Y. Qiu, W. Y. Zou, Y. Qian and H. L. Zhu, *RSC Adv.*, 2015, **5**, 23767–23777.
28 M. D. Vitorovic-Todorovica, A. Eric-Nikolic, B. Kolundzija, E. Hamel, S. Ristic, I. O. Juranic and B. J. Drakulic, *Eur. J. Med. Chem.*, 2013, **62**, 40–50.
29 D. Kumar, N. M. Kumar, K. Akamatsu, E. Kusaka, H. Harada and T. Ito, *Bioorg. Med. Chem. Lett.*, 2010, **20**, 3916–3919.
30 M. Liu, P. Walairat, S. L. Croft, A. L. Tan and M. L. Go, *Bioorg. Med. Chem.*, 2003, **11**, 2729–2738.
31 V. Peyrot, D. Leynadier, M. Sarrazin, C. Briand, A. Rodriquez, J. M. Nieto and J. M. Andreu, *J. Biol. Chem.*, 1998, **264**, 21296–21301.
32 V. Peyrot, D. Leynadier, M. Sarrazin, C. Briand, M. Menendez, J. Laynez and J. M. Andreu, *Biochemistry*, 1992, **31**, 11125–11132.
33 N. J. Lawrence, R. P. Patterson, L. L. Ooi, D. Cook and S. Ducki, *Bioorg. Med. Chem. Lett.*, 2006, **16**(22), 5844–5848.
34 D. J. Kerr, E. Hamel, M. K. Jung and B. L. Flynn, *Bioorg. Med. Chem.*, 2007, **15**(9), 3290–3298.
35 K. G. Pinney, A. D. Bounds, K. M. Dingeman, V. P. Mocharla, G. R. Pettit, R. Bai and E. Hamel, *Bioorg. Med. Chem. Lett.*, 1999, **9**(8), 1081–1086.
36 G. R. Pettit, S. B. Singh, M. R. Boyd, E. Hamel, R. K. Pettit, J. M. Schmidt and F. Hogan, *J. Med. Chem.*, 1995, **38**, 1666–1672.
37 R. B. Ravelli, B. Gigant, P. A. Curmi, I. Jourdain, S. Lachkar, A. Sobel and M. Knossow, *Nature*, 2004, **428**, 198–202.
38 R. C. Elderfield, I. S. Covey, J. B. Geidushek, W. L. Meyer, A. B. Ross and J. H. Ross, *J. Org. Chem.*, 1958, **23**, 1749–1753.
39 L. S. Goodman, M. M. Wintrobe, W. Dameshek, M. Goodman, A. Z. Gilman and M. T. McLennan, *J. Am. Med. Assoc.*, 1946, **132**(3), 126–132.
40 A. Sankaraperumal, J. Karthikeyan, A. Nityananda Shetty and R. Lakshmisundaram, *Polyhedron*, 2013, **50**, 264–269.
41 S. Anitha, J. Karthikeyan and A. Nityananda Shetty, *Indian J. Chem.*, 2013, **52A**, 45–50.
42 A. Sankaraperumal, A. Nityananda Shetty and J. Karthikeyan, *Synth. React. Inorg., Met.-Org., Nano-Met. Chem.*, 2015, **45**(9), 1318–1326.
43 F. Xianwen, Z. Lizhen, C. Zhao, Y. Meipan and Y. Bingqin, Synthesis, Crystal structures and antitumor activity of novel nitrogen mustard linked chalcones, *Chin. J. Org. Chem.*, 2013, **33**, 523–529.
44 T. Liljefors and N. L. Allinger, *J. Am. Chem. Soc.*, 1976, **98**(10), 2745–2749.
45 Y. S. Xue and X. D. Gong, *THEOCHEM*, 2009, **901**, 226–231.
46 Y. Xue, J. Mou, Y. Liu, X. Gong, Y. Yang and L. An, *Cent. Eur. J. Chem.*, 2010, **8**(4), 928–936.
47 J.-C. Lien and L.-J. Huang, *J. Chin. Chem. Soc.*, 2004, **51**, 847–852.
48 S. Ducki, D. Rennison, M. Woo, A. Kendall, J. F. D. Chabert, A. T. McGown and N. J. Lawrence, *Bioorg. Med. Chem.*, 2009, **17**, 7711–7722.
49 A. R. Chaudhuri, P. Seetharamalu, P. M. Schwarz, F. H. Hausheer and R. F. Luduena, *J. Mol. Biol.*, 2000, **303**, 679–692.
50 Y. Luo, K. M. Qiu, X. Lu, K. Liu, J. Fu and H. L. Zhu, *Bioorg. Med. Chem.*, 2011, **19**, 4730–4738.
51 B. F. Ruan, X. Lu, J. F. Tang, Y. Wei, X. L. Wang, Y. B. Zhang, L. S. Wang and H. L. Zhu, *Bioorg. Med. Chem.*, 2011, **19**, 2688–2695.
52 G. A. M. Jardim, T. T. Guimaraes, M. C. F. R. Pinto, B. C. Cavalcanti, K. M. de Farias, C. Pessoa, C. C. Gatto, D. K. Nair, I. R. R. Namboothiri and E. N. de Silva Junior, *Med. Chem. Commun.*, 2015, **6**, 120–130.
53 K. Bacharaju, S. J. Reddy, S. Sivan, S. J. Tangeda and V. Manga, *Bioorg. Med. Chem. Lett.*, 2012, **22**, 3274–3277.
54 X. Fang, B. Yang, Z. Cheng, M. Yang, N. Su, L. Zhou and J. Zhou, *Arch. Pharm. Chem. Life Sci.*, 2013, **346**, 292–299.
55 V. Sharma, A. Chaudhary, S. Arora, A. K. Saxena and M. P. S. Ishar, *Eur. J. Med. Chem.*, 2013, **69**, 310–315.
56 Y. Qian, G. Ma, Y. Yang, K. Cheng, Q. Zheng, W. Mao, L. Shi, J. Zhao and H. Zhu, *Bioorg. Med. Chem.*, 2010, **18**, 4310–4316.
57 S. Ducki, R. Forrest, J. A. Hadfield, A. Kendall, N. J. Lawrence, A. T. McGown and D. Rennison, *Bioorg. Med. Chem. Lett.*, 1998, **8**(9), 1051–1056.
58 N. J. Lawrence, A. T. McGown, S. Ducki and J. A. Hadfield, *Anti-Cancer Drug Des.*, 2000, **15**, 135–141.
59 A. Tenderholt, *QMForge: A Program to Analyze Quantum Chemistry Calculations, Version, 2.3.2*, http://qmforge.sourceforge.net.
60 N. Nagarajan, G. Velmurugan, G. Prabhu, P. Venuvanalingam and R. Renganathan, *J. Lumin.*, 2014, **147**, 111–120.
61 N. Nagarajan, A. Prakash, G. Velmurugan, N. Shakti, M. Katiyar, P. Venuvanalingam and R. Renganathan, *Dyes Pigm.*, 2014, **102**, 180–188.
62 N. Nagarajan, G. Velmurugan, G. Prabhu, P. Venuvanalingam and J. Renganathan, *J. Photochem. Photobiol., A*, 2014, **284**, 36–48.
63 G. Velmurugan, S. A. Vedha and P. Venuvanalingam, *RSC Adv.*, 2014, **4**, 53060–53071.
64 G. M. Sheldrick, *Acta Crystallogr., Sect. A: Found. Crystallogr.*, 2008, **A64**, 112–122.
65 L. J. Farrugia, *J. Appl. Crystallogr.*, 1997, **30**, 565.
66 A. L. Spek, *J. Appl. Crystallogr.*, 2007, **36**, 7–13.
67 M. Dickson and J. P. Gagnon, *Nat. Rev. Drug Discovery*, 2004, **3**, 417–429.
68 C. A. Lipinski, F. Lombardo, B. W. Dominy and P. J. Feeney, *Adv. Drug Delivery Rev.*, 2001, **46**(1–3), 3–26.
69 M. J. Frisch, G. W. Trucks, H. B. Schlegel, G. E. Scuseria, M. A. Robb, J. R. Cheeseman, G. Scalmani, V. Barone, B. Mennucci, G. A. Petersson, H. Nakatsuji, M. Caricato, X. Li, H. P. Hratchian, A. F. Izmaylov, J. Bloino, G. Zheng, J. L. Sonnenberg, M. Hada, M. Zhara, K. Toyota, R. Fukuda, J. Hasegawa, M. Ishida, T. Nakajima, Y. Honda, O. Kitao, H. Nakai, T. Vreven, J. A. Montgomery, J. E. Peralta, F. Ogliaro, M. Bearpark, J. J. Heyd, E. Brothers, K. N. Kudin, V. N. Staroverov, R. Kobayashi, J. Normand, K. Raghavachari, A. Rendell, J. C. Burant, S. S. Iyengar, J. Tomasi, M. Cossi,

N. Rega, J. M. Millam, M. Klene, J. E. Knox, J. B. Cross, V. Bakken, C. Adamo, J. Jaramillo, R. Gomperts, R. E. Stratmann, O. Yazyev, A. J. Austin, R. Cammi, C. Pomelli, J. W. Ochterski, R. L. Martin, K. Morokuma, V. G. Zakrzewski, G. A. Voth, P. Salvador, J. J. Dannenberg, S. Dapprich, A. D. Daniels, Ö. Farkas, J. B. Foresman, J. V. Ortiz, J. Cioslowski and D. J. Fox, *Gaussian 09, Rev. B., 01*, Gaussian, Inc., Wallingford, CT, 2009.

70 A. D. Becke, *J. Chem. Phys.*, 1993, **98**, 5648.

71 A. D. Becke, *Phys. Rev. A: At., Mol., Opt. Phys.*, 1988, **38**, 3098.

72 J. P. Perdew, *Phys. Rev. B: Condens. Matter Mater. Phys.*, 1986, **33**, 8822.

73 C. Lee, W. Yang and R. G. Parr, *Phys. Rev. B: Condens. Matter Mater. Phys.*, 1988, **37**, 785.

74 A. E. Reed, L. A. Curtiss and F. Weinhold, *Chem. Rev.*, 1988, **88**, 899.

75 T. Langer and E. Krovat, *Curr. Opin. Drug Discovery Dev.*, 2003, **6**, 370–376.